Materials Research Proceedings 41 (2024) 2534-2543 https://doi.org/10.21741/9781644903131-279

Applicability of productivity enhanced sinking-EDM of cemented carbide forming tools for bipolar plates

PETERSEN Timm[1,a*], VOIGTS Herman[1,b], HERRIG Tim[1,c] and BERGS Thomas[1,2,d]

[1]Manufacturing Technology Institute (MTI) of RWTH Aachen University, Campus-Boulevard 30, 52074 Aachen, Germany

[2]Fraunhofer Institute for Production Technology IPT, Steinbachstraße 17, 52074 Aachen, Germany

[a]t.petersen@mti.rwth-aachen.de, [b]h.voigts@mti.rwth-aachen.de, [c]t.herrig@mti.rwth-aachen.de, [d]t.bergs@mti.rwth-aachen.de

Keywords: Cemented Carbide, Sinking-EDM, Coining, Freeform Surface, Bipolar Plate

Abstract. The present research uses a previously published method to reduce the duration to machine cemented carbide forming tools by SEDM. Because of the forming setup a relatively thick sheet metal was used, which is why a forming simulation was conducted beforehand to achieve a valuable design, derived from bipolarplates, to observe wear in the forming experiments.

Introduction

One of the enablers to reduce the amount of greenhouse gas emissions in the transportation sector are fuel cells [1]. The large number of bipolarplates needed in a fuel cell and their tight tolerances make them cost drivers [2,3]. Therefore, it is of importance to improve the manufacturing process to reduce costs and to enhance their degree of effectiveness [4]. This will allow for a more sustainable and economically acceptable transformation to green transportation.

The effectiveness is enhanced with a rectangular flowfield geometry, which is responsible for the distribution of the working media. This geometric demand and the tight tolerances call for tool materials of high rigidity that are able to transfer their shape to the workpiece accurately and repeatably [5]. A class of materials, which is able to withstand the large compressive stresses needed to comply with these demands are cemented carbides. Another advantageous property of cemented carbides, regarding the challenging tool geometries found in the filigree channel structure of the flowfield, is their large resistance to wear. The high hardness of cemented carbides requires machining technologies like electrical discharge machining (EDM). Its thermophysical working principle enables for machining workpieces independently of their mechanical properties. Albeit, there are two concerns regarding the EDM of cemented carbides, which are subject of several recent publications. On the one hand, the machining of cemented carbides is less productive in comparison to steel and on the other hand the thermal removal mechanism can cause cracks and flaws that would reduce the longevity of the workpieces – in this case the forming tools. Previously conducted research has described the effects sinking EDM has on the surface integrity of cemented carbides [6]. Additionally, the resulting workpiece functionality has been examined [6,7]. Finally, the process has been altered in order to reduce machining duration and the corresponding effect on the surface integrity has been found to be negligible [8]. As a final step in this series of research, the altered sinking EDM process is compared to the standard process in a real application. Due to the necessity of large scale tests, the forming of bipolarplates was chosen as the application test case. It is therefore an additional aim of this research to investigate the wear mechanisms of cemented carbide forming tools that were machined by sinking EDM.

Punch design and preliminary simulations

For wear testing, a die setup from [9] was used. However, the process was designed for coining thus only the embossing pattern is of relevance. The punch contour was used for guidance in an existing tool setup. A bipolarplate geometry, provided by Fraunhofer IPT, Aachen was used as a reference for the present experiments. Additionally, two features were added to allow for an evaluation of different radii and coining heights, cf. Fig. 1.

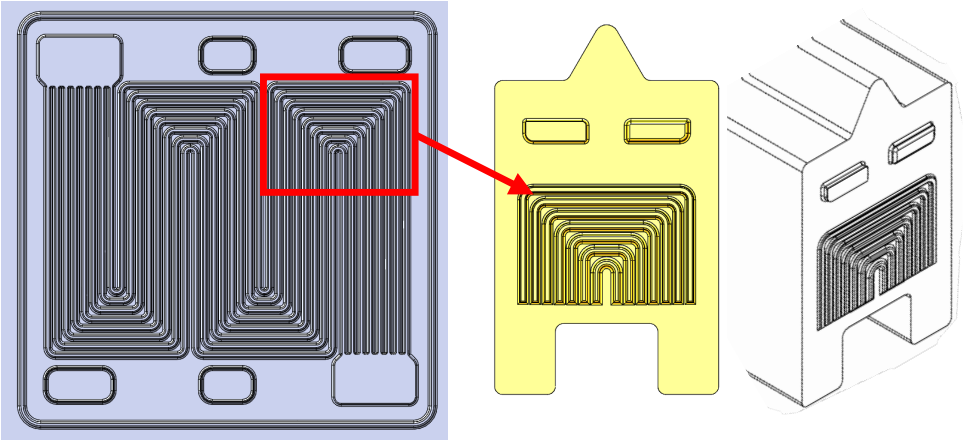

Fig. 1: Reference bipolarplate (left), punch design with section of the flowfield of the bipolarplate (centre) and isometric view of the embossing pattern (right).

In order to reduce the tool life time, an analogue setup for tribological testing of the channel structures of the embossing pattern was used with the sheet metal strip thyssenkrupp precidur (AISI 52100/1.3505) with a thickness of 3.7 mm and UTS of 660 MPa. This ensures increased wear rates at a similar load collective with significantly higher stress levels (contact pressure: 600 MPa) compared to bipolarplate pressing (contact pressure: 85 MPa). The material was selected due to its similar tribological behavior compared to thin foil used for bipolarplates such as AISI 316L/1.4404. However, the coining setup, led to the question whether the cavity between the channels of the flowfield would fill properly to see friction on the flanks of the channel structure. The software Forge 4.0 was used to design material flow and stresses in the embossing pattern. Fig. 2 displays the equivalent stress for a directly derived flowfield geometry.

As shown in the top view, the stresses are the highest around the corners. In the enlarged cross sectional view the colored workpiece material does not reach the punch contour. The height of the

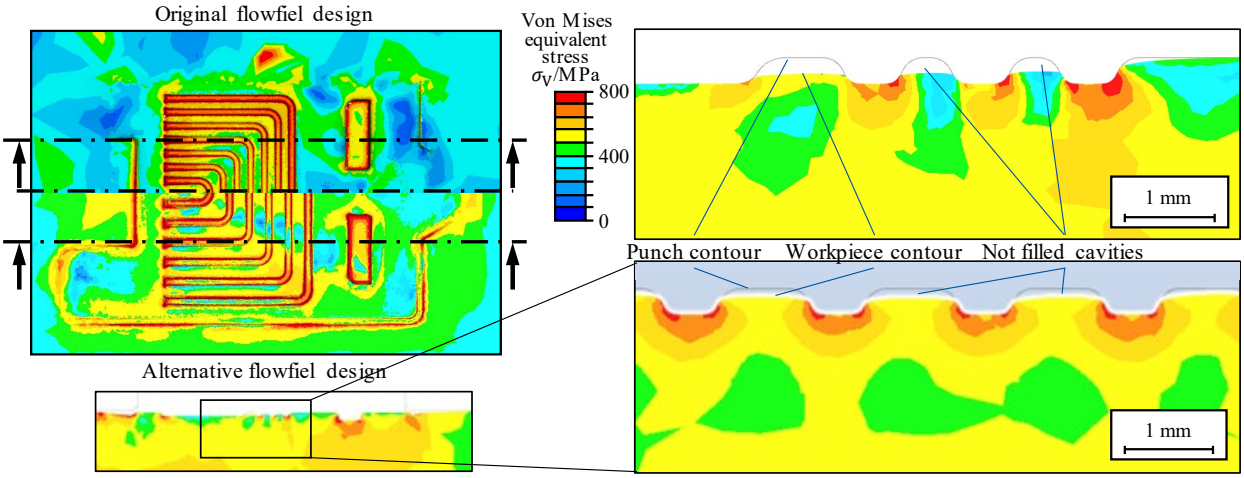

Fig. 2: Simulation results for both geometries with top view (top left), cross sectional view (bottom left) and enlarged cross sectional view of original (top right) and alternative design (bottom right).

channels in the flowfield of the workpiece only reach 45 % of the designated height. Because of the curvature of the material within the channels, there is even less material in the vicinity of the flanks of the flowfield of the punch. In order to improve the material filling between the channels, the distance between channels was increased. The number of channels was reduced to six. The simulation was repeated with the adapted geometry. It is apparent that the contour was sufficiently filled to create material flow over the radii of the channel pattern. The height of the channels in the workpiece reached 78 % of the designated height. The material appears to create enough friction thus wear around the corners and flanks in analogy to flowfield drawing.

The final geometry that was used for the derivation of the sinking-EDM tool is displayed in Fig. 3. The features 1 and 2 have a height of 0.7 mm, whereas the flowfield only has a height of 0.3 mm. Both features have a bottom radius of 0.25 mm, feature 1 a head radius of 0.05 mm and feature 2 has a head radius of 0.3 mm. All the corners have different radii as well to allow for a differentiation between wear mechanisms. The channels 1 to 6 all have the same corner radius, which was taken from the initial geometry. They have increasing head radii by an increment of 0.02 mm, starting at 0.1 mm for channel 1 until 0.2 mm for channel 6. The bottom radii increase accordingly, however, starting at 0.2 mm for channel 1 up to 0.3 mm for channel 6. The channel height and different radii were chosen according to research conducted regarding the formability of foils used for bipolarplate manufacturing [10].

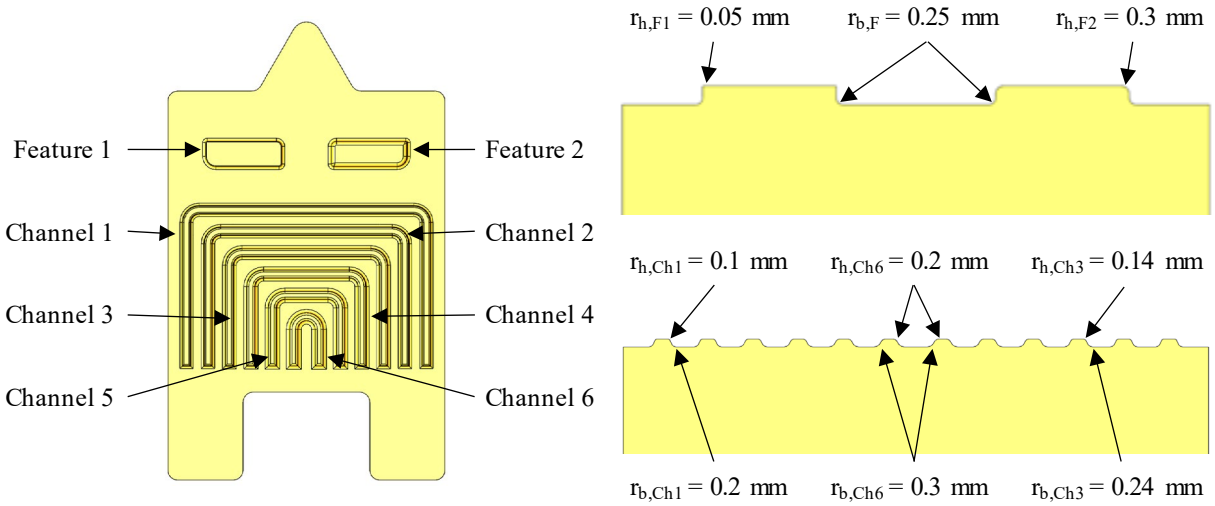

Fig. 3: Final punch design with a distance between the flow field channels of 1.7 mm (left), cross sectional view of the features with corresponding radii (top right) and cross sectional view of the flowfield with exemplary channel head and bottom radii (bottom right).

Machining of cemented carbide punches

The punches were machined from EDM-blocks of the tungsten carbide grade Ceratizit CTF35 (average grain size 0.8 µm, Cobalt-content 17.5 wt-%). First the outer shape of the punches was cut via wire-EDM on a GFMS P550 with 4 trim cuts up to a surface roughness of Ra = 0.4 µm. Additionally, the guide for the forming tool has been cut in a PM steel on the same machine tool. Subsequently, the desired shape was machined via sinking-EDM on a GFMS Form 2000 VHP. The machining sequence and the machining parameters are displayed in Fig. 4. Even though the electrode material was chosen as copper-tungsten, with 30 wt.-% copper, the wear was expected to be of a magnitude that prevents a proper shape transfer. Therefore, three electrodes were milled with a machining duration of 16 h each. In order to spread the wear evenly, roughing and super-finishing started with punch 1 and the intermediate finishing operation started reversely with punch 2. The necessity of this altered sequence can also be seen from the machining duration of machining steps 1 and 2. Because of the significant linear wear of approximately 15 %, electrode 1

was 0.14 mm shorter before the start of machining of punch 2 and was hence significantly faster. Due to the additional wear, punch 2 was missing approximately 0.21 mm from the original machining depth of 1 mm. This difference was compensated with the finishing operation. As indicated in Fig. 4 (right), the roughing steps are conducted again with both subsequent electrodes. This ensures an equal spread of the wear and that both punches reach the desired machining depth. The wear of the electrodes was measured with the sinking EDM machine tool after machining both punches and was 0.21 mm, 0.04 mm and 0.01 mm for the roughing, finishing and super-finishing electrode respectively.

		Punch 1	Punch 2
Roughing	Machining step	1	2
	Electrode	1	1
	Time / min	435	384
Finishing	Machining step	4	3
	Electrode	2	2
	Time / min	72	155
Super-Finishing	Machining step	5	6
	Electrode	3	3
	Time / min	71	70

Roughing

Finishing

Super-Finishing

I / A	T / µs	P / µs	U / V	SBOX	Ra / µm
4.7	7	15	-200	74	1.58
4.7	5	15	-200	69	1.26
4.7	4	10	-200	67	1
3.2	3.2	7	-200	246	0.79
2.8	3.2	4.5	-200	219	0.63
2.6	3.2	3.6	-200	199	0.5
2.6	2	3.6	-200	196	0.4
1.2	2	3.6	-170	195	0.31
1.2	1.6	3.6	170	195	0.25
0.8	1.6	3.6	120	193	0.2

Fig. 4: Description of machining sequence with machining duration (left) and machining parameters with resulting surface roughness (right).

The machining parameters were adjusted according to the approach described in [8]. However, the expected reduction of machining duration was not observed in this setup. Since this was attributed to the wear, which caused different machining durations for both punches, a comparative study according to the setup described in [8] was conducted with the material relevant for this investigation. It was found that the machining time was reduced by 12 %, which is in the order of magnitude that was expected. Additionally, the machining duration and the wear in the present research are relatively high, because of the filigree structures that were machined. In order to make sure that the shape with its varying radii is properly transferred from the electrodes to the punches, the undersize was only 0.05 mm per side. However, the wear of the electrodes was stronger than expected, which is why the final surfaces were not all the same. A measurement with the laser scanning microscope Keyence VK-X has revealed that the bottom surfaces of the punches reached a surface roughness of Ra = 0.2 µm. In contrast, the head surfaces of the flow channels of the punches have only reached a surface roughness of Ra = 0.5 µm. This is exactly the surface roughness that was reached after the finishing operation. Because the electrodes have worn differently in these different areas, the super-finishing operation was not anymore conducted on the head surface. This is illustrated by Fig. 5, where the part of the electrode that machines the bottom of the workpiece is the first to interact with the workpiece. With ongoing machining, this part is worn, even when the rest of the electrode has not yet started to machine. Only after the height difference in the electrode has been surpassed, the wear takes place in all regions quasi equally. After machining, the workpiece resembles the negative of the shape of the worn electrode and when a new electrode is used, there is a gap between the areas that were machined with a lesser worn electrode than those that were machined with parts of the electrodes that were subject to more wear. Even after using several electrodes, this effect can still be seen, since it is repeated with subsequent electrodes, however, with another magnitude.

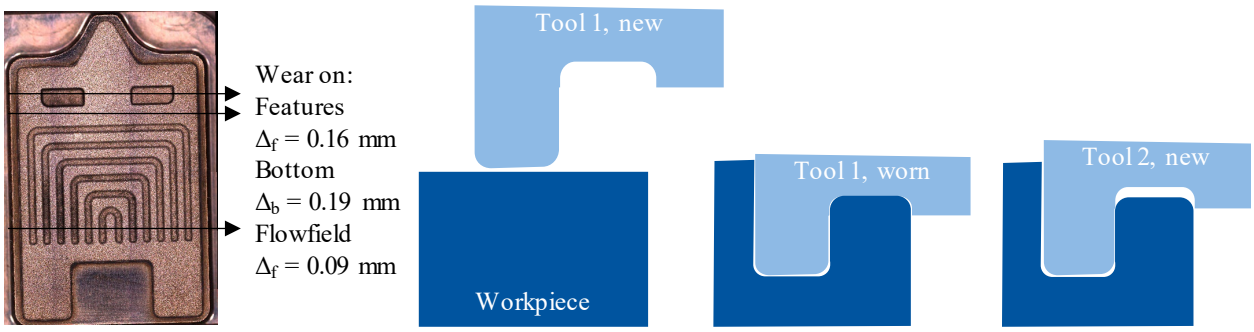

Fig. 5: Worn roughing electrode with corresponding linear material reduction (left) and corresponding error propagation (right): Electrode and workpiece before machining, worn electrode after first machining operation with corresponding workpiece and same workpiece with new, not worn electrode.

The previously described effect can also be seen in the images taken via scanning electron microscopy (SEM). Fig. 6 depicts one of the flow channels which has the described features. On the one hand the bottom surfaces as well as the flank surfaces appear to be smooth. On the other hand, the head surface of the channel appears to be a lot rougher. Additionally, there are some single craters, which are significantly larger than those that make up the surrounding surfaces. These craters probably result from a concentration of the electric field on corners and the corresponding ignition of discharges with higher energies in earlier machining steps with a larger gap width. These single craters can be seen frequently on the corners of all machined features and might have been removed, if the frontal undersize of the electrodes had been adjusted according to the occurring wear.

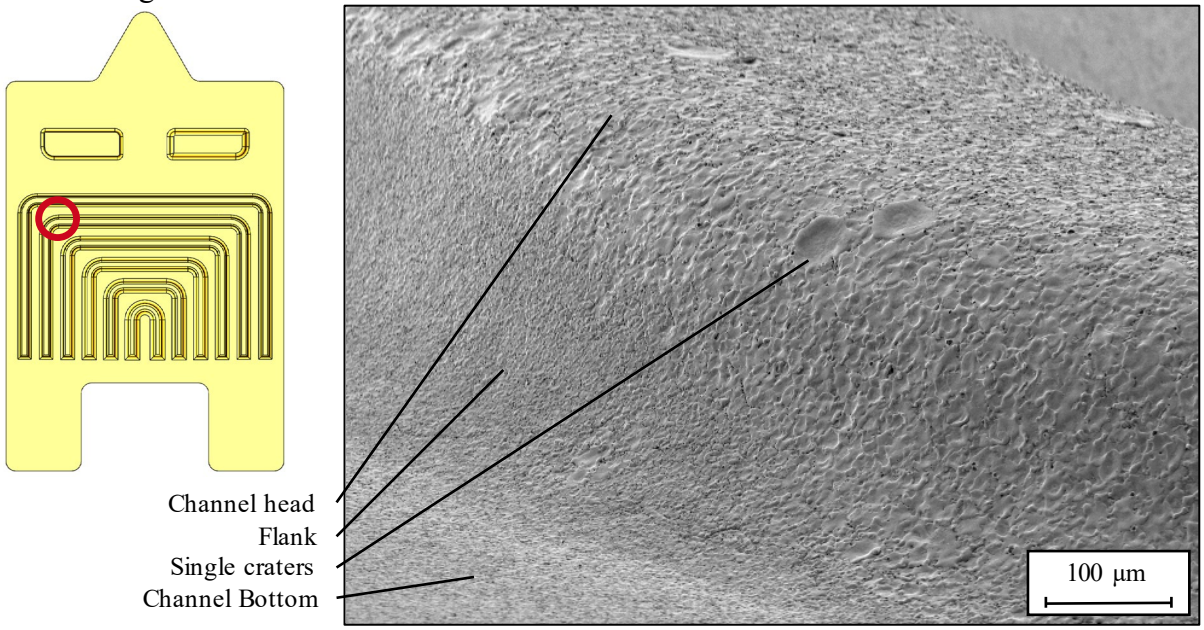

Fig. 6: Image for orientation (top left), SEM image of the second flow channel on the second punch.

Experimental setup for coining tests

The profile was coined into the sheet metal strip in an automatic stamping process for wear testing. A full coil of the beforementioned material AISI 52100/100Cr6 with thickness 3.7 mm and UTS of 660 MPa was used for a total of 7360 strokes. The experiments were performed on a servomechanical blanking press Feintool XFT 2500speed at stroke rates between 15 min^{-1} and 45 min^{-1}. In order to coin the full profile into the sheet metal, the die was replaced with a rigid

anvil instead of a counterholder. Fig. 7 shows the tool used for the experiments. Coining took place in the top dead center (TDC) of the underneath drive. The stroke length was calibrated in the beginning for a full penetration of the sheet metal according to the process design from the simulations. The die setup was a 2-up die with two cavities. Punch 1 was EDMed with a reference technology whereas punch 2 was manufactured with the adapted technology (see above).

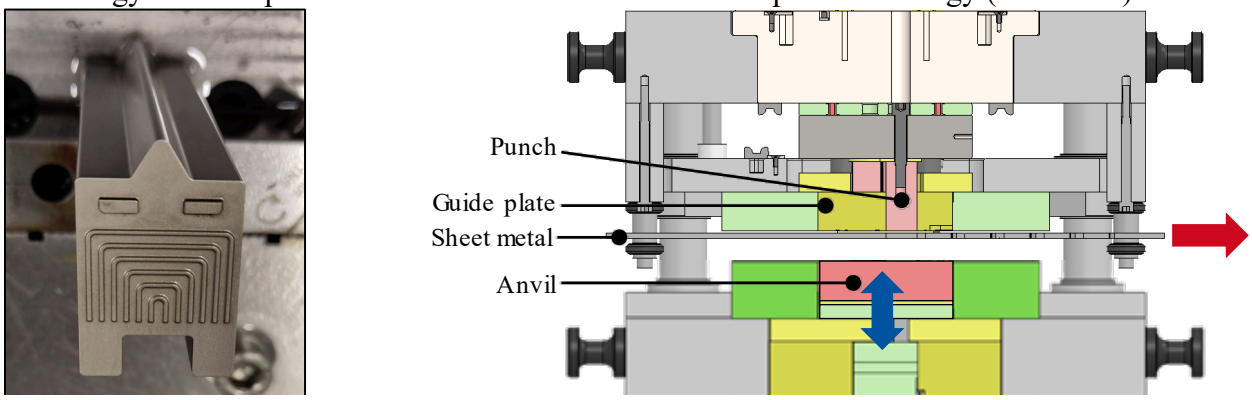

Fig. 7: Punch 1 after SEDM (left) and tool setup with blue arrows indicating the movement of the underneath drive and red indicating the feed direction of the sheet metal (left).

Coined specimens were extracted every 500 strokes for further analysis of forming results and eventual traces resulting from wear on the punch. For this, the coined surface was measured and evaluated using laser scanning microscopy. The tool state was analyzed using scanning electron microscopy (SEM) in initial state, after 1000 strokes and after the total 7360 strokes. The quality of the S-EDMed surface in all radii and surfaces was assessed visually. Traces of adhering sheet metal as well as cracks and surface wear indications were looked for.

Results and Discussion

During the first 50 strokes, feature 1 broke from both punches. As mentioned above, the small radii were designed as edge cases. The small head radius and the flank experience tensile load during the return stroke because of clamping between the feature and sheet metal according to [9]. The tensile load causes crack formation in the bottom radius of the feature as can be seen on the non-broken features 2 in Fig. 8. Another explanation might be shear load on the features away from the middle of the strip due to lateral material flow in the compression phase.

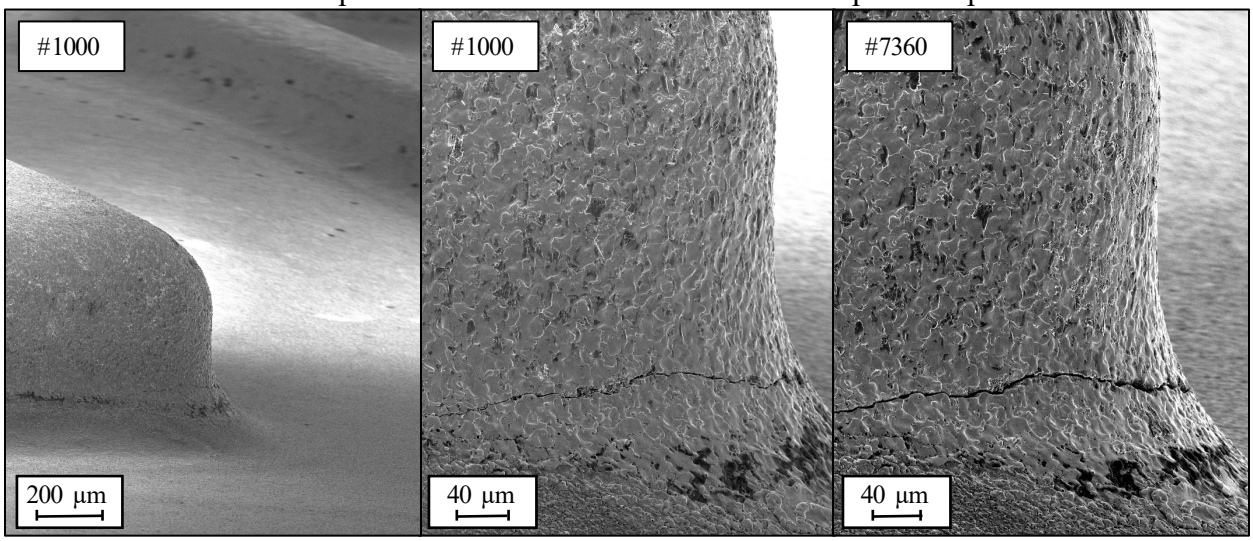

Fig. 8: Overview for orientation of corner on feature 2 of punch 1(left) and detailed view of crack development on the bottom radius after 1000 strokes (left and centre) and after 7360 strokes (right).

Materials Research Proceedings 41 (2024) 2534-2543 https://doi.org/10.21741/9781644903131-279

Another major event during the forming tests was the partial demolition of channel 1 on punch 1, which was machined with the reference technology. The breakage did indicate itself with some major cracks along channel 1. Fig. 9 highlights the imprint of these cracks on a specimen after 750 strokes. Furthermore, after another 2000 strokes channel 1 broke off partially as visible by the specimen after 2750 strokes. The final stage of the demolition process was reached after 4000 strokes. Another ~3300 strokes were conducted without additional fractures.

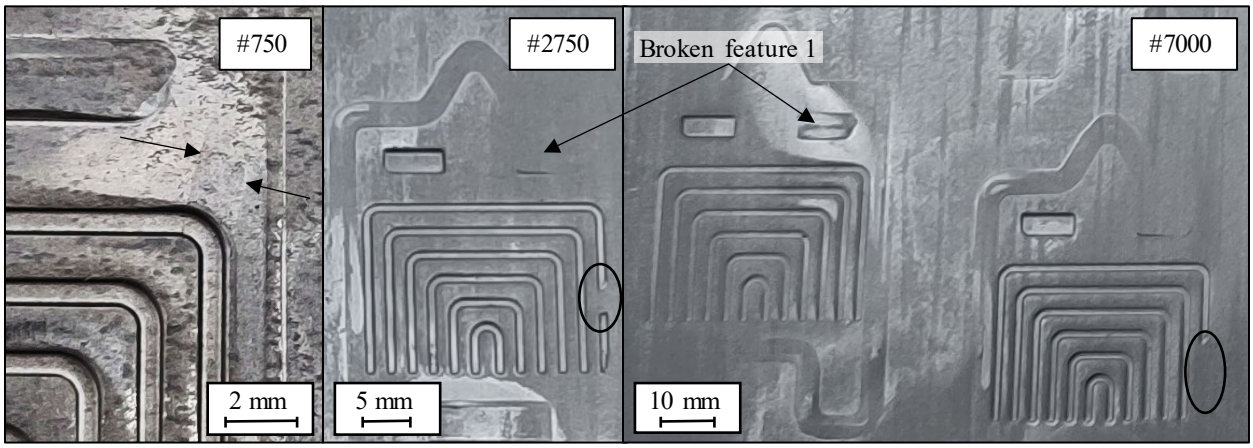

Fig. 9: Detailed view of the imprint of the cracks developing on punch 1 after 750 strokes (left), first specimen with the imprint of the first stage of the partially breakage of channel 1 (centre) and specimen with imprint of the intact punch 2 and the imprint of the final breakage state of punch 1 after 7000 strokes (right).

Fracture of features and tribological wear are a result of a high compressive load collective. In previous work regarding cemented carbide wear during stamping, such fractures were explained by tensile and bending stresses during the stripping phase. High stresses in the coining phase create spring back of the formed surfaces causing a clamping situation between the coining features and the sheet metal. Additional lateral stresses due to material flow towards the strip edges as a result of upsetting the sheet metal are an explanation for the observed fractures. The sheet metal is compressed by the punch force and blankholder force, see Fig. 10.

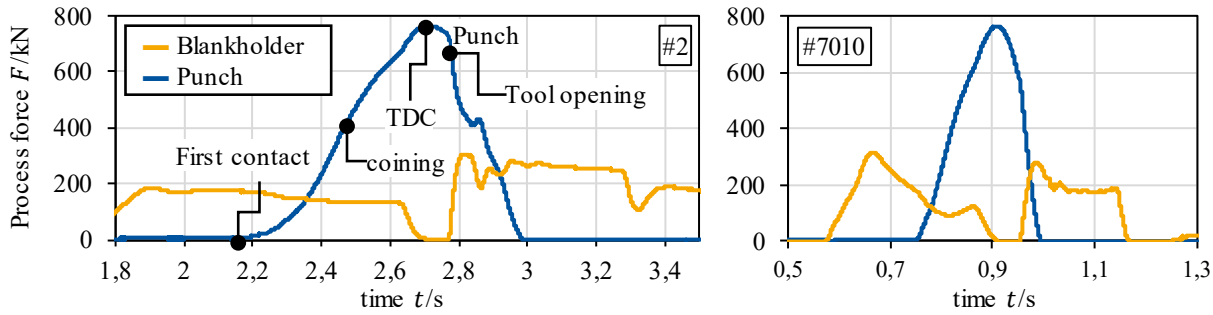

Fig. 10: Process forces during coining representing high compressive load collective on channel pattern for the second stroke (left) and the 7010th stroke (right).

The axial load on both punches adds to almost 800 kN which equals about 600 MPa contact stress. The contact stress is in the range of the UTS of the sheet metal (660 MPa). The axial load is responsible for wear to be observed on the channel flanks. After 1000 strokes, the rate has been increased from 15 to 45 min^{-1} to increase wear.

A profilometer was used to measure the depth of the imprinted profile of extracted workpieces. Fig. 11 depicts one exemplary sheet metal strip and the measurements of the depths of the imprints of both punches. The red lines on the left show the position and direction of the measurements, approximately 1 mm from the bottom end of the flow fields. As visible in the graphs on the right-

hand side of Fig. 11, both positions yielded different depths. The flowfield on the right-hand side of the sheet metal strip, whose corresponding data is depicted in the upper graph, averaged to a depth of 0.255±0.045 mm. The other flowfield only reached a depth of 0.184±0.022 mm, averaged over all channels and investigated specimens. The reason for this difference was not attributed to different punch heights, since the position of the punches was swapped after 1000 strokes. However, this explains the slight drift in all measurements from specimen 1000 to specimen 1250. The reason for the difference between the two positions is suspected to be found in the tool setup. As depicted in Fig. 7, the punches are positioned behind one another. This is also indicated by the positions of the red lines in Fig. 11. The blue arrow indicates the feed direction of the sheet metal strip. After one stroke is conducted, the relatively small feed of the sheet metal strip causes the guide plate to press down on the flowfield that has already been imprinted on the left-hand side. This might have caused the filigree structure of the flowfield to be compressed.

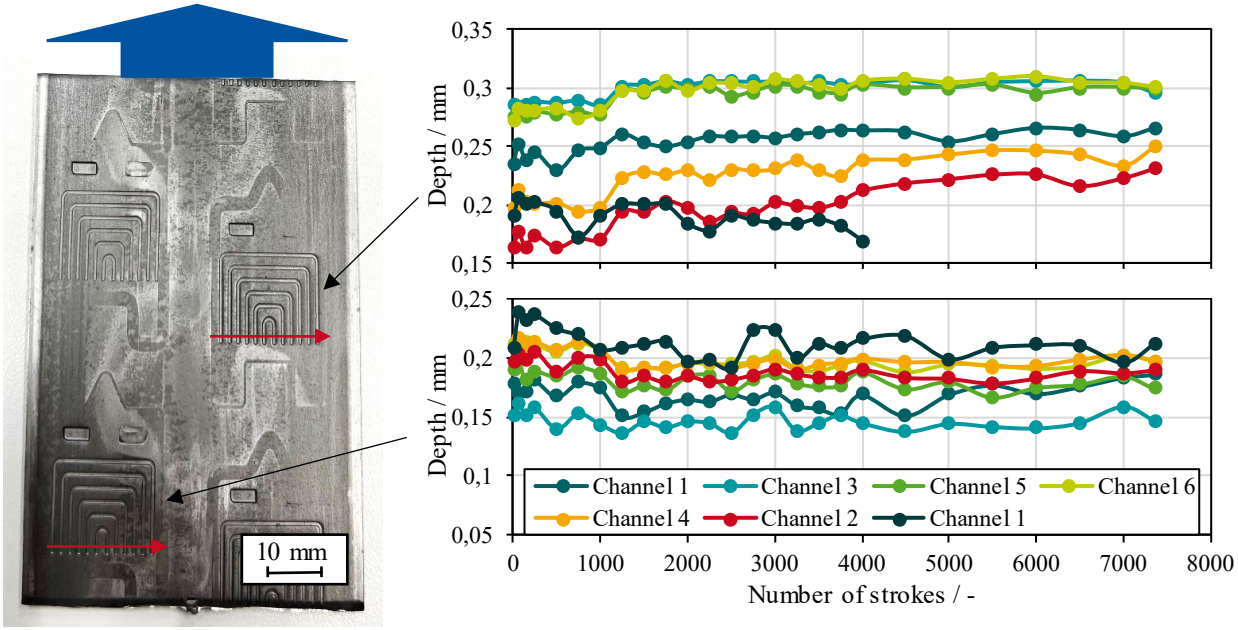

Fig. 11: Sheet metal strip with imprinted flowfield and Feature 2 as well as red line indicating position of profile measurements (left) and depths of the indicated channels as a function of the number of strokes (right).

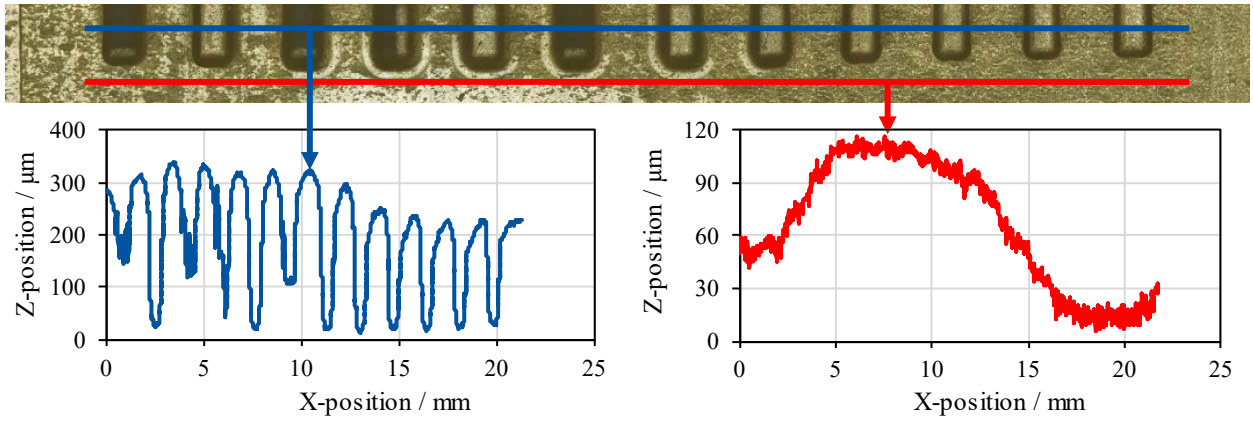

Fig. 12: Laser scanning microscope image of sheet metal strip with imprinted flowfield with red and blue lines indicating positions of profile measurements (top), profile taken on the blue line containing the flowfield (bottom left) and profile taken on the red line indicating the shape of the sheet metal strip (bottom right).

The measurements of the right-hand side flowfield reveal that not all channels, but only channels 3, 5 and 6, reached the expected depth of 0.3 mm, cf. Fig. 11. One possibility is that the larger radii towards the middle of the flowfield allowed for a less restricted material flow. However, the measurements taken with a laser scanning microscope reveal, that the metal sheet has a profiled surface, see Fig. 12. The magnitude of the bulge is the same as that of the missing depth. The measurements of channel 1 on the right-handed side, in the upper graph of Fig. 11, also indicate the beforementioned partial fracture of channel 1. The depths of the channels closest to the broken one appear to become larger after it broke off. Overall, the profile measurements show that the imprint is even better than expected by the simulation. This might be caused by the pocket effect of the EDMed surface and the resulting constant supply of lubricants in the contact area as previously discussed by [11].

Besides fractures, wear characteristics were analyzed using SEM-imaging. Fig. 13 presents the tool surface of the channel pattern after 7360 strokes. The microstructure of the EDMed as well as alteration due to tribological load and adhesion of sheet metal on the surface.

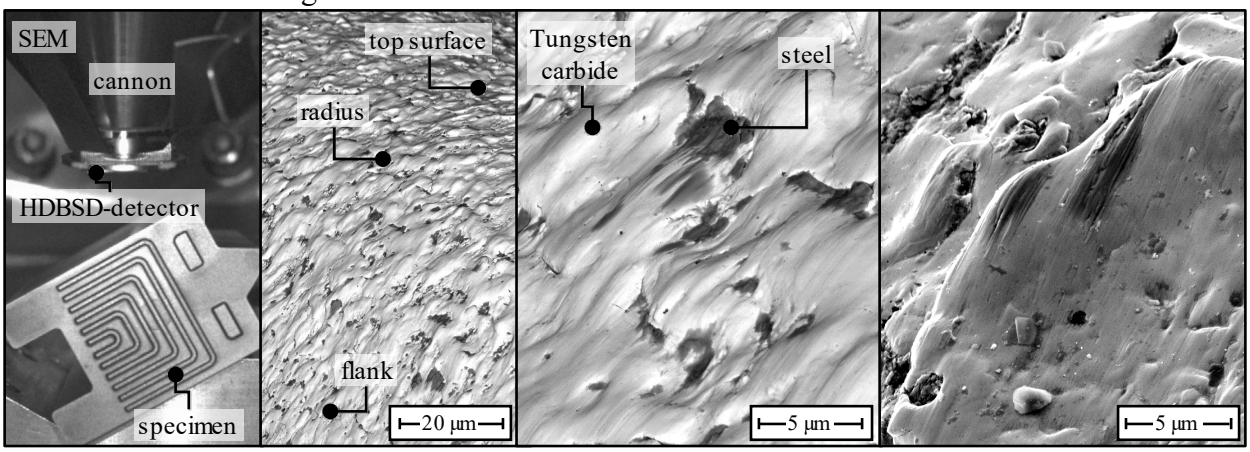

Fig. 13: SEM images of tribologically loaded head radius of channel pattern.

Overall, the surface only shows minor characteristics of abrasive wear. A slight texture in sliding direction can be seen on the SEM images of the head radius and flanks. The abrasive wear does not exceed a slight surface polish. Moreover, sheet metal steel was found adhering on the surface and mechanically disposed in valleys of the surface profile. The adhesion is no wear as to the definition as material loss on the technical surface. However, adhesion indicates that the tribological load on the surface was increased.

Conclusion

The present paper has conducted one step towards a possible new manufacturing route for bipolarplates. First of all, it has shown that the previously published method to enhance the productivity of sinking EDM of cemented carbides is transferable to different cemented carbide grades. Hence, this method is a valuable tool to improve the machining of cemented carbides in general. Furthermore, it was stated that this method does not harm the surface integrity of the workpieces. The comparison of the two punches did not indicate an increased number of flaws for the alternative machining technology. In contrast, the punch which was machined with the reference technology experienced major fractures. However, the fracture of the feature is attributed to an overly ambitious geometry whereas the fracture of the flowfield channel to the occurrence of shearing and lateral movement and forces of the sheet metal, due to its thickness. On the other hand, the examination of the tribological wear has not shown any significant issues. A slight polishing of the punch and some adhesion of the sheet metal was observed. In general, these findings indicate that cemented carbide tools are suited for the filigree structures present in bipolarplates and that even areas with non-optimal surface roughness are able to withstand the

tremendous loads. Moreover, the analysis of the profile has revealed that the imprint is even better than expected by the simulation, which would be helpful to create a proper sealing of the bipolarplates and increase their degree of effectiveness.

Acknowledgements
The authors thank the German Research Foundation (DFG) for funding the DFG project BE 2542/42-2: "Analysis of the discharge-dependent surface integrity of cemented carbide forming dies machined by sinking EDM and its influence on the tribological characteristics and the resulting fatigue behaviour" (project number 290130034) and the Bundesminsterium für Wirtschaft und Klimaschutz (BMWK, Federal Ministry for Economic Affairs and Climate Action; Projectnumber 20N2204D – KeyTech2GreenPower).

References

[1] C. Baum, H. Janssen, C. Brecher et al. (2021) The Relevance of Fuel Cells for Mobility Applications. Discussion Paper. Fraunhofer-Gesellschaft, Aachen. https://doi.org/10.24406/IPT-N-633591

[2] M. Miotti, J. Hofer, C. Bauer (2017) Integrated environmental and economic assessment of current and future fuel cell vehicles. Int J Life Cycle Assess 22:94–110. https://doi.org/10.1007/s11367-015-0986-4

[3] B. D. James, J. M. Huya-Kouadio, C. Houchins et al. (2018) Fuel Cell Vehicle Cost Analysis: Annual Progress Report - Hydrogen and Fuel Cell Programm 2017. V.E.5

[4] L. Peng, P. Yi, X. Lai (2014) Design and manufacturing of stainless steel bipolar plates for proton exchange membrane fuel cells. International Journal of Hydrogen Energy 39:21127–21153. https://doi.org/10.1016/j.ijhydene.2014.08.113

[5] U. Engel, J. Groenback, C. Hinsel (2011) Tooling solutions for challenges in cold forging. Umformtechnik

[6] T. Bergs, T. Petersen, U. Tombul et al. (2020) Analysis of the Influence of Surface Integrity of Cemented Carbides Machined by Sinking EDM on Flexural Fatigue. Procedia CIRP 87:456–461. https://doi.org/10.1016/j.procir.2020.02.096

[7] T. Petersen, U. Küpper, T. Herrig et al. (2021) Fracture Toughness and Tribological Properties of Cemented Carbides Machined by Sinking Electrical Discharge Machining. ESAFORM 2021:13. https://doi.org/10.25518/esaform21.1518

[8] T. Petersen, U. Küpper, A. Klink et al. (2022) Discharge energy based optimisation of sinking EDM of cemented carbides. Procedia CIRP 108:734–739. https://doi.org/10.1016/j.procir.2022.03.113

[9] H. Voigts, R. Hild, A. Feuerhack et al. (2021) Investigation of Failure Mechanisms of Cemented Carbide Fine Blanking Punches by Means of Process Forces and Acoustic Emission. In: Forming the Future. Springer, Cham, pp 1173–1187. https://doi.org/10.1007/978-3-030-75381-8_98

[10] D. Qiu, L. Peng, P. Yi et al. (2018) Flow channel design for metallic bipolar plates in proton exchange membrane fuel cells: Experiments. Energy Conversion and Management 174:814–823. https://doi.org/10.1016/j.enconman.2018.08.070

[11] T. Petersen, U. Küpper, T. Herrig et al. (2023) Coefficient of friction of cemented carbides machined by sinking EDM. Materials Research Proceedings 28:1765–1774. https://doi.org/10.21741/9781644902479-191